ELSEVIER

Journal of Magnetism and Magnetic Materials 191 (1999) 61–71

Journal of magnetism and magnetic materials

Enhanced perpendicular magnetic anisotropy in chemically long-range ordered (0 0 0 1)Co_xPt_{1-x} films

M. Maret[a,*], M.C. Cadeville[a], A. Herr[a], R. Poinsot[a], E. Beaurepaire[a], S. Lefebvre[b], M. Bessière[b]

[a]*Institut de Physique et Chimie des Matériaux de Strasbourg, Groupe d'Etude des Matériaux Métalliques, UMR 46 CNRS-ULP, 23 rue du Loess, F-67037 Strasbourg, France*

[b]*Laboratoire pour l'Utilisation du Rayonnement Electromagnétique, CNRS-CEA-MEN, Bât 209d, F-91405 Orsay, France*

Received 18 March 1998; received in revised form 18 September 1998

Abstract

Chemical long-range ordering along the growth direction has been observed in mostly HCP $Co_{80}Pt_{20}$ films grown on a Ru(0 0 0 1) buffer by the molecular beam epitaxy technique. Such ordering, strongly dependent on both the growth temperature and the crystalline quality of the alloy film, is revealed to enhance perpendicular magnetic anisotropy in HCP films. Pt segregation effect at the advancing surface, allowed by dominant surface diffusion, would be the driving force for promoting such uniaxial long-range ordering during the MBE process. Yet, ex situ annealing treatments performed at temperatures similar to the growth temperature have shown that the MBE-promoted chemical ordering, different from those found in the bulk $L1_2$- or DO_{19}-type ordered A_3B compounds, is metastable in agreement with theoretical calculations.

PACS: 61.10.F; 61.55.H; 75.30.G; 75.60; 75.70

Keywords: Co-Pt alloy films; Structure; Chemical order; Magnetic anisotropy

1. Introduction

The growth of epitaxial alloy films is a promising way of producing chemically ordered phases, with respect to the conventional metallurgical techniques for bulk alloys. Among this class of materials, the Co_xPt_{1-x} films are among the most studied ones, since they are potential magneto-optical recording media for blue laser recording [1]. For the study of magnetic anisotropy and its relation to structure, Co–Pt is also a well-appropriate system. The Co–Pt phase diagram displays at high temperatures a disordered FCC solid solution over the whole composition range, and at lower temperatures two FCC $L1_2$ ordered phases around the composition $CoPt_3$ and Co_3Pt and one tetragonal $L1_0$ ordered phase around the equiatomic composition. The FCC Co_xPt_{1-x} alloys are

*Correspondence address. Universität Konstanz, Fakultät für Physik, Jakob-Burckhardt-Strabe 29, Postfach X915, D-78457 Konstanz, Deutschland. Tel: +49-7531-88-2036; fax: +49-7531-88-3895; e-mail: mireille.maret@uni-konstanz.de.

0304-8853/99/$ – see front matter
PII: S0304-8853(98)00373-4

ferromagnetic at room temperature for Pt content up to 85 at% and interestingly, the ordered phases, CoPt and $CoPt_3$, have Curie temperatures lower than those of the corresponding disordered phases. For example, the Curie temperature of the $CoPt_3$ ordered compound is 170 K lower than that of the disordered phase [2], which is attributed to the absence of CoCo nearest neighbor pairs in the ordered $L1_2$ compound [3].

In epitaxial (1 1 1) $CoPt_3$ films, it was shown that the development of perpendicular magnetic anisotropy, strongly dependent on the growth temperature, is correlated with the existence of anisotropic structural order effects, characterized by preferential heteroatomic pairs out of the film plane, promoted by the molecular beam epitaxy (MBE) technique [4]. The highest uniaxial anisotropy about 1 MJ/m^3 was found in a film grown around 690 K [5,6]. In contrast, the occurrence of the $L1_2$-type isotropic chemical ordering, favored by an increase of the deposition temperature around 800 K and characterized by (1 1 1) planes of identical $CoPt_3$ composition, gives rise to a disappearance of perpendicular magnetic anisotropy. Recently, angle-dependent X-ray magnetic circular dichroism measurements in these films have shown that the microscopic origin of the magneto-crystalline anisotropy is related to 3d and 5d orbital moment anisotropies, such as the out-of-plane components of the orbital moments are higher than the in-plane components [7,21].

The growth of CoPt films on an MgO(0 0 1) substrate at 780 K leads to the formation of a $L1_0$ tetragonal ordered phase with the *c*-axis along the surface normal, which presents strong perpendicular anisotropy [8]. Let us recall that in a fully $L1_0$-type ordered film the stacking sequence along the [0 0 1] easy direction of magnetization consists of alternate pure Co and pure Pt planes, while along the hard axes [1 0 0] and [0 1 0] all the planes have the equiatomic composition; therefore, all nearest-neighbor CoPt pairs are oriented out of the (0 0 1)CoPt film plane. As also found in $CoPt_3$ films, the existence of strong perpendicular magnetic anisotropy stems from the hybridization between Co atoms of large magnetic moment and Pt atoms of strong spin–orbit coupling, preferentially along the surface normal.

On the Co-rich side, chemical long-range ordering (LRO) along the growth direction was found in epitaxial films. The first evidence was in 1000 Å thick $Co_{77}Pt_{23}$ films deposited on sapphire(0 0 0 1) with a 10 Å Pt buffer; such ordering was correlated with the emergence of a new peak at 3.2 eV photon energy in magneto-optical spectra [9]. More recently, ordering effects were found in 500 Å thick $Co_{82}Pt_{18}$ films deposited on mica(0 0 1) with a 150 Å Ru buffer, in which the stacking sequence is predominantly HCP; such ordering along the surface normal clearly increases perpendicular magnetic anisotropy [10].

In this paper, we present a detailed structural study of the Co-rich films grown on (0 0 0 1)Ru buffer, from X-ray diffraction measurements. Their magnetic properties, studied by means of SQUID magnetometry and polar Kerr effects, are also reported and discussed in relation with their structure. Futhermore, the contributions of surface and volume diffusion during the co-deposition process to the formation of anisotropic chemical ordering and associated perpendicular magnetic anisotropy are discussed, together with the decrease of chemical ordering observed after ex situ anneal treatments.

2. Experimental procedures

Co_xPt_{1-x} films of 400–500 Å thickness were deposited at different temperatures ranging from 500 to 750 K in a 10^{-10} Torr vacuum onto a 150 Å Ru(0 0 0 1) buffer grown at 900 K on a mica(0 0 1) substrate. These alloy films were covered by a 20 Å protective Pt layer deposited at room temperature. Electron gun sources were used for both Co and Pt with deposition rates in the range 0.05–0.2 Å/s monitored by two quartz balances. In our UHV deposition chamber, up to six mica substrates, 3 cm in diameter each, can be fixed to a holder. First the six Ru buffer layers were prepared simultaneously. Then, using an appropriate disk of 60° aperture masking five substrates, alloy films could be grown at different temperatures successively, by starting with the sample grown at the highest temperature. Nevertheless, the advantage of preparing a series of six samples is somewhat attenuated. On the one

hand annealing effects can occur in the first deposited films. On the other hand, though the same deposition rates are used, the film composition can vary from one mica position to another with respect to both Co and Pt sources; such composition gradient observable in the first series, was subsequently eliminated by increasing the oscillation angle of the sample holder from 180 to 330° during co-deposition. The substrate temperature was measured with a K-type thermocouple located close to the holder leading to an uncertainty estimated at 20 K.

The RHEED patterns observed along the azimuths [1 0 $\bar{1}$ 0] and [1 1 $\bar{2}$ 0] revealed the crystalline quality of the alloy films on the Ru(0 0 0 1) buffer with the following epitaxial relationships:

Co_xPt_{1-x} (0 0 0 1) [1 0 $\bar{1}$ 0] ∥ Ru(0 0 0 1) [1 0 $\bar{1}$ 0],

Co_xPt_{1-x} (1 1 1) [1 1 $\bar{2}$] ∥ Ru (0 0 0 1) [1 0 $\bar{1}$ 0].

The X-ray diffraction measurements were performed: (i) on a high-resolution(HR) X-ray Philips diffractometer using a four-Ge(2 2 0) crystal monochromator providing a pure Cu K_{α_1} parallel beam; three types of measurements were collected, θ–2θ symmetric reflection scans, rocking curves in symmetric and asymmetric geometries, (ii) on a D500 Siemens diffractometer with monochromatic Co K_α beam of higher intensity but of lower resolution, for measuring weak superstructure peaks in θ–2θ geometry.

X-ray measurements were also carried out at the laboratoire pour l'utilisation du rayonnement electromagnétique (LURE) in Orsay, France, on the DIF4C diffractometer below the Co–K absorption edge at an energy of 7501 eV ($\lambda = 1.653$ Å). Measurements in both reflection and transmission geometries were done in samples previously oriented and whose substrates were cleaved down to a thickness of 30–80 μm. Furthermore, diffraction rods were recorded by measuring the diffracted intensity as a function of the normal component of the scattering vector, with the in-plane component fixed at $4\pi/d_{nn}^{\parallel}$ ($d_{nn}^{\parallel}$ is the in-plane nearest-neighbor distance). Along this rod, the Bragg peaks characteristic of both HCP and FCC stacking sequences are well separated. From their integrated intensities, the volume fractions of each phase can be determined.

Basically, symmetric reflection measurements give information on the spacing between planes stacked along the growth direction and the associated coherence length, while symmetric transmission measurements provide the in-plane lattice parameters and the lateral coherence length.

The magnetic properties of the alloy films were studied at 300 K by measuring the polar and longitudinal Kerr effects using a laser diode ($\lambda = 670$ nm) with the applied field up to 1.3×10^3 kA/m, and at 30 K using a SQUID magnetometer with the applied field up to 5.6×10^3 kA/m. For the SQUID measurements, the dimensions of the samples were 4×4 mm^2 and cleaved down to a thickness of ~10–30 μm to minimize the contribution of the mica substrate. The effective magnetic anisotropies ($K_{eff} = K_u - 0.5\,\mu_0 M_s^2$) were deduced from the area enclosed between the parallel and perpendicular magnetization hysteresis curves measured at 30 K.

3. Results

3.1. X-ray diffraction measurements

The main diffraction peaks of the alloy layer, buffer and substrate are shown in Fig. 1 for four samples among three different series. The chosen samples were the most relevant for studying the relationships between their structure and magnetic properties. The solid curves were measured in θ–2θ reflection geometry on the high-resolution diffractometer and the dashed curves are the rocking curves around the (0 0 0 2) or (1 1 1)CoPt and (0 0 0 2)Ru peaks. For the samples a and b of a first series and the sample c of a second series, the alloy films were grown at 690, 500 and 650 K, respectively, their thickness controlled by low-angle X-ray reflectivity measurements is close to 500 Å and their Co composition checked by electron probe microanalysis is around 80 at%. For the sample d of a third series, the alloy film grown at 700 K is only 400 Å thick and somewhat poorer in Co with 75 at% Co content. The main peak of the alloy film refers to a 0 0 0 2 or 1 1 1 reflection depending on its majority stacking sequence (HCP or FCC). The normal coherence lengths, $L_\perp = \lambda/2\Delta\theta_{h\,k\,l} \cos\theta_{h\,k\,l}$,

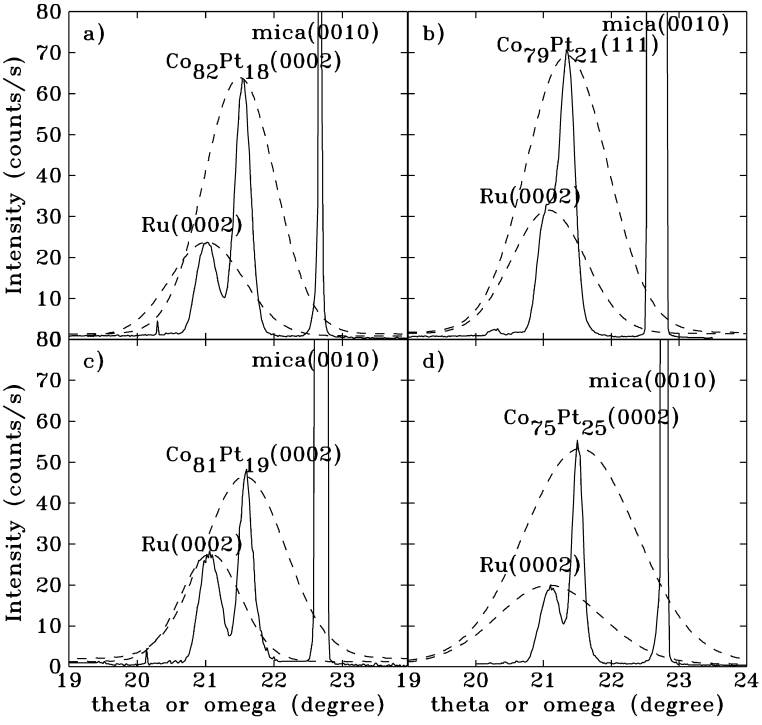

Fig. 1. θ–2θ X-ray diffraction scans (—) and ω-scans around the 0 0 0 2 (or 1 1 1)Co_xPt_{1-x} and 0 0 0 2 Ru reflections (- - -) measured on a HRXRD Philips diffractometer ($\lambda = 1.5406$ Å) for four Co_xPt_{1-x} films of three different series: (a and b) are two samples of series 1 grown at 690 and 500 K, (c) one sample of series 2 grown at 650 K; and (d) one sample of series 3 grown at 700 K.

$h\,k\,l = 0\,0\,2$ or $1\,1\,1$, together with the widths of the rocking curves are reported in Table 1.

The most interesting feature observed for some of these alloy films is the existence of a superstructure peak in the θ–2θ patterns around 1.5 $Å^{-1}$ which is a fingerprint of chemical LRO along the growth direction. As shown in Fig. 2, the intensity of this peak, referred to as a 0 0 0 1 reflection, increases with the growth temperature T_g, from 500 to 690 K. As precised further by the calculation of a chemical LRO parameter, S, the chemical modulation along the growth direction is favored by increasing T_g from 500 to 690 K. However, such a peak was observed neither in the film d grown at 700 K (not shown in Fig. 2), nor in three other samples of the third series grown at 600, 650 and 750 K and this result will be discussed hereafter.

Fig. 3 shows the high-order 0 0 4 reflections for sample a which has the most intense superstructure peak. The Co_xPt_{1-x} alloy peak is asymmetric and can be decomposed into two Gaussian components. Based on the h-rods diffraction rods described later, the smallest one refers to the 2 2 2 reflection of minority FCC stacking and the largest one to the 0 0 0 4 reflection of majority HCP stacking. Such a decomposition shows that HCP stacking is about 0.015 Å denser than FCC stacking. In Table 1, are thus reported the out-of-plane parameters for both HCP and FCC stackings when the two components can be solved reliably.

The 1 0 1 diffraction rod measurements lead to a complete separation between the reflections coming from HCP and FCC stackings, and therefore to a better determination of the volume fractions of two stackings. Fig. 4 displays the 1 0 1 diffraction rods referred to the HCP phase along which are superimposed the $0\,0\,\bar{2}$ and $1\,1\,\bar{1}$ reflections of FCC stacking and the $\bar{1}\,1\,1$ and 0 0 2 reflections of twinned FCC. The volume fractions of HCP and FCC(+twin) stackings, reported in

Table 1
Main structural and magnetic properties of the four Co_xPt_{1-x} alloy films grown on a Ru(0 0 0 1) buffer. $L_\perp$ and $L_\parallel$ normal and in-plane coherent lengths; $\Delta\omega^{0\,0\,0\,2}_{CoPt}$ and $\Delta\omega^{0\,0\,0\,2}_{Ru}$ full-widths at half-maximum of the rocking curves around the 0 0 0 2(1 1 1)Co_xPt_{1-x} and 0 0 0 2 Ru reflections; %HCP volume fraction of HCP stacking; c^{HCP} and a^{HCP} lattice parameters of HCP stacking; S chemical order parameter; $a_\perp^{FCC}$ and $a_\parallel^{FCC}$ lattice parameters of FCC stacking deduced from the 1 1 1 and 0 $\bar{2}$ 2 peak positions; $(c/a)^*$ deviation from the ideal ratio of HCP stacking equal to $\sqrt{8/3}$; $a_\perp^{FCC}/a_\parallel^{FCC}$ deformation of FCC stacking; M_s saturation magnetization; K_{eff} effective magnetic anisotropy and $K_u = K_{eff} + 0.5\mu_0 M_s^2$ uniaxial magnetic anisotropy.

Alloy Comp.	Growth Temp. (K)	$L_\perp$ (Å) $L_\parallel$ (Å)	$\Delta\omega^{0\,0\,0\,2}_{CoPt}$ (°) $\Delta\omega^{0\,0\,0\,2}_{Ru}$ (°)	% HCP S	c_{HCP} (Å) a_{HCP} (Å)	$a_\perp^{FCC}$ (Å) $a_\parallel^{FCC}$ (Å)	$(c/a)^*$ $a_\perp^{FCC}/a_\parallel^{FCC}$	M_s (kA/m)	K_{eff} (MJ/m^3) K_u (MJ/m^3)
$Co_{82}Pt_{18}$	690	185	1.1	86	4.18	~3.645	0.985	1245	1.6
(a-series1)		230	1.2	0.54	2.6	3.675	0.992		2.6
$Co_{79}Pt_{21}$	500	190	1.4	7	–[a]	3.66	–	1215	−0.2
(b-series1)		140	1.2	0	~2.61	3.685	0.993		0.7
$Co_{81}Pt_{19}$	650	205	1.4	42	4.18	3.635	0.988	1260	0.05
(c-series2)		210	1.1	0.1	2.59	3.66	0.993		1
$Co_{75}Pt_{25}$	700	280	1.9	90	4.205	–	0.985	1105	0.8
(d-series3)		190	1.8	0	2.615	3.7	–		1.5

[a]The missing lattice parameters are related to the insufficient contributions of the minority phase to the diffracted intensities.

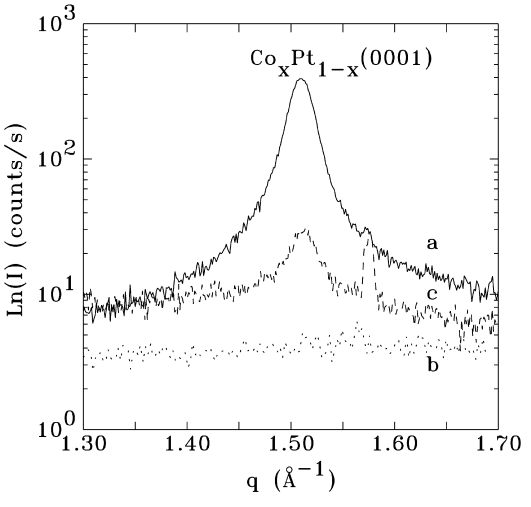

Fig. 2. X-ray diffracted intensities as a function of the scattering vector $q = 4\pi \sin\theta/\lambda$ around the 0 0 0 1 reflection measured, on a D500 Siemens diffractometer, for three samples grown at 690 K (—), 650 K (- - -) and 500 K (....) described in Fig. 1.

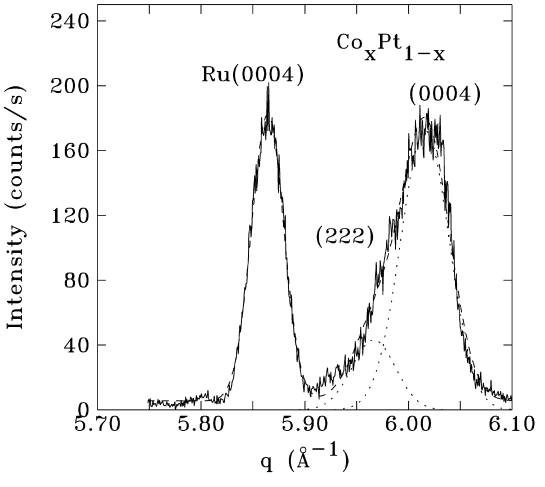

Fig. 3. X-ray intensities around the 0 0 0 4, 2 2 2 Co_xPt_{1-x} and 0 0 0 4 Ru reflections measured on a D500 diffractometer for the $Co_{82}Pt_{18}$ alloy grown at 690 K (sample a). The dotted curves are the two Gaussian components attributed to the majority HCP and minority FCC phases.

Table 1, are deduced from the integrated intensities of these peaks, normalized by the square of their respective structure factors. Up to 700 K, an increase of the deposition temperature favors HCP stacking, while beyond 700 K, as shown by Harp et al. [9], FCC stacking becomes predominant in these films.

The crystalline quality of the HCP stacking, characterized by the width of the 1 0 1 reflections is clearly better in sample a than in sample d. The monocrystalline quality of the alloy film is directly dependent on the Ru buffer, as indicated by the widths of the rocking curves around the 0 0 0 2 CoPt and Ru reflections given in Table 1.

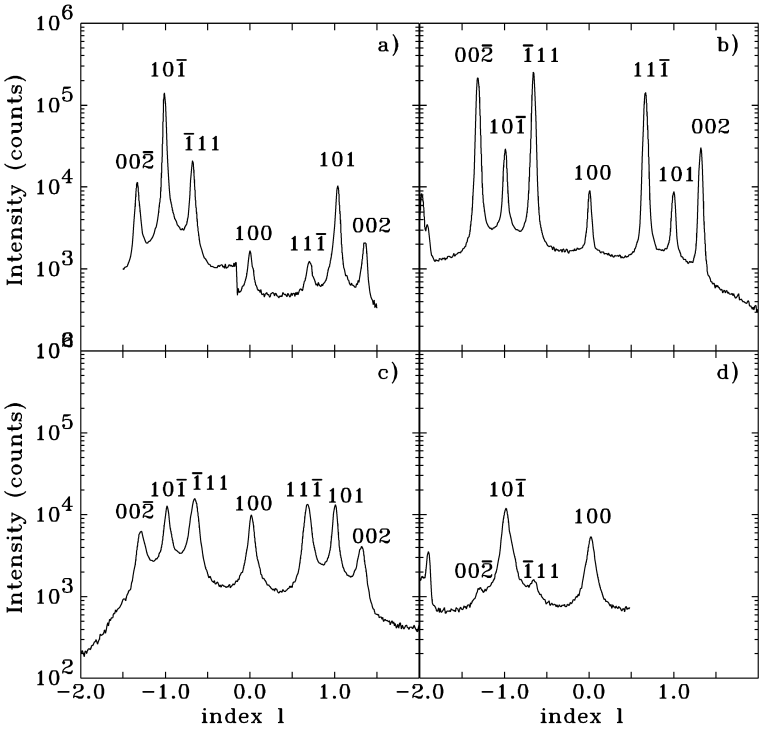

Fig. 4. 1 0 l diffraction rods referred to the HCP phase measured on the DIF4C diffractometer at LURE(Orsay) for the four samples presented in Fig. 1; along this rod are superimposed the 0 0 $\bar{2}$ and 1 1 $\bar{1}$ for the FCC phase and $\bar{1}$ 1 1 and 0 0 2 for the twinned FCC.

Chemical long-range order along the growth direction can be characterized by a parameter S deduced from the ratio of the $I_{0\,0\,0\,1}$ and $I_{0\,0\,0\,2}$ diffracted intensities, corrected for absorption and Lorentz polarization factor. It can be written as $S = (\tau_1 - \tau_2)/2x_{\mathrm{Pt}}$, where τ_1 and τ_2 are the occupancy rates of Pt atoms on the Pt-rich and Pt-poor alternate (0 0 0 1) planes, with $\tau_1 + \tau_2 = 2x_{\mathrm{Pt}}$; S is then equal to 1 as one layer is occupied by only Co atoms (i.e. $\tau_2 = 0$). Chemical ordering in these films is really uniaxial since no $\frac{1}{2}$ 0 0 and $\frac{3}{2}$ 0 0 reflections, signatures of in-plane chemical ordering, were detected from synchrotron radiation measurements in symmetric transmission geometry. The values of the in-plane lattice parameter a^{HCP} and the lateral coherence length $L_{\parallel}$ of the HCP phase deduced from the 1 0 0 CoPt peak are reported in Table 1. No separation is observed between the 0 $\bar{2}$ 2 FCC and 2 2 0 HCP reflections. The in-plane lattice parameter extracted from these reflections, which for the HCP phase is in good agreement with that deduced from HCP 1 0 0 reflection, also holds for the FCC phase (labelled $a_{\parallel}^{\mathrm{FCC}}$ in Table 1).

From Table 1, the deviations $(c/a)^*$ from the ideal HCP stacking smaller than 1 reveal that the HCP stacking in the alloy films is under strain. Similarly, as shown by the deviation from the FCC ideal stacking characterized by $a_{\perp}/a_{\parallel}$ ratio, the FCC stacking is also slightly compressed. The S parameters of samples a and c do not fit completely with the growth temperature dependence of the chemical LRO parameter found in Ref. [9], which can be attributed to the uncertainty of temperature measurements. However, as shown in Fig. 5, our data (except for series 3) display the same increase of S with the HCP volume fraction, as that reported by Harp et al. [9].

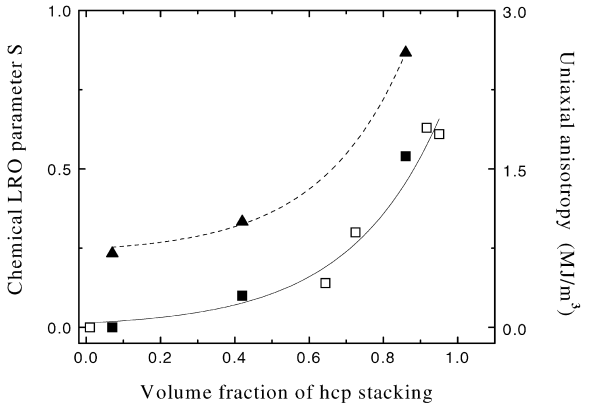

Fig. 5. Chemical long-range order parameter S (■) and uniaxial magnetic anisotropy K_u (▲) as a function of the HCP volume fraction for the films a, b and c grown on Ru(0 0 0 1). For comparison, the S values for $Co_{77}Pt_{23}$ films grown on sapphire(0 0 0 1) measured by Harp et al. [9] are also displayed (□).

Nevertheless, even if the formation of HCP stacking and chemical ordering occur in the same growth temperature range, chemical ordering in the minority FCC phase cannot be excluded. This question was recently elucidated from digital processing of FCC areas in cross-section HRTEM images of sample a and 2D-Fourier transformation. Chemical ordering in the minority FCC phase was indeed confirmed by the presence of an intermediate peak referring to a $\frac{1}{2}\frac{1}{2}\frac{1}{2}$ reflection along the [1 1 1] growth direction [11]. Chemical ordering along the growth direction was also observed by X-ray diffraction in an epitaxial (1 1 1)$Co_{50}Pt_{50}$ film grown at 690 K and adopting only FCC stacking.

Coming back to the absence of a 0 0 0 1 peak for the alloy films of series 3 grown in a temperature range, where chemical ordering was expected, we can emphasize the larger out-of-plane (1.9°) and in-plane mosaicities (3°) measured for this series compared to those measured for sample a (1.1 and 1.5°, respectively). Hence, the lateral and normal extents of alternate Co-rich and Co-poor plane stacking is reduced by the presence of a great number of steps, which would prevent constructive interference effects between second-neighbor (0 0 0 1) planes, which are at the origin of the 0 0 0 1 superstructure peak in the X-ray pattern.

3.2. Magnetic measurements

Fig. 6 shows the parallel and perpendicular magnetization hysteresis loops measured at 30 K for the four samples. The magnetic behavior of these samples changes drastically with their structure, since for samples a and d, mostly HCP, the easy axis of magnetization is along the growth direction [0 0 0 1], while for sample b, mostly FCC, the easy axis lies in the film plane and for sample c, consisting of equivalent HCP and FCC volume fractions, an intermediate behavior is observed.

The saturation magnetization and the magnetic anisotropy energies, K_{eff} and K_u, deduced from the SQUID hysteresis loops are listed in Table 1. The effective anisotropy found for the chemically long-range ordered HCP film (sample a, 1.6 MJ/m^3) is comparable to the value measured in [Co(3 Å)/Pt(10 Å)] multilayers [12] and is twice larger than the value of the chemically disordered HCP film (sample d, 0.8 MJ/m^3).

Besides, as shown in Fig. 5, the uniaxial anisotropies, K_u, display the same HCP volume fraction dependence as the chemical parameter S. Therefore, the magneto-crystalline anisotropy increases with both the HCP volume fraction and the uniaxial chemical LRO. It is well established that the origin of the magneto-crystalline anisotropy is the spin–orbit interaction which induces an orbital moment coupling the total (spin + orbital) magnetic moment to the crystal axes. The enhancement of the perpendicular anisotropy in the LRO HCP films results clearly from the uniaxial symmetry of the HCP phase and from the 3d–5d hybridization preferentially along the c-axis and the large 5d spin–orbit coupling of Pt atoms.

Also, it is worth noting that the K_u value of the chemically disordered HCP film (sample d) of 1.5 MJ/m^3 is significantly larger than the value of pure HCP Co equal to 1 MJ/m^3. This result suggests the existence of anisotropic chemical short-range order, such that the CoPt nearest-neighbor pairs are preferentially oriented along the surface normal, leading to an enhancement of perpendicular anisotropy compared to HCP Co. As already done for $CoPt_3$ films [4], XAFS measurements at the Pt-L_3 edge using the polarization of synchrotron

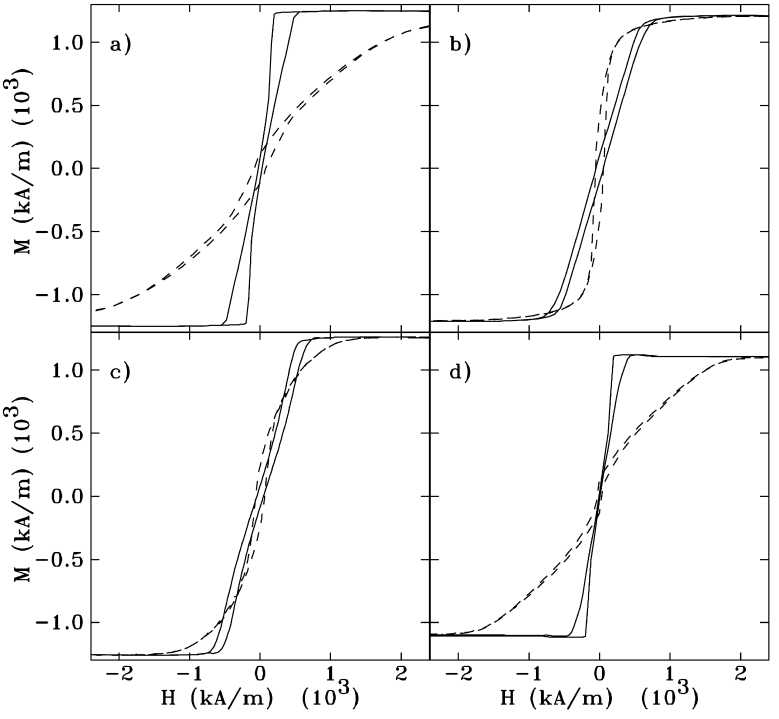

Fig. 6. Magnetization hyteresis loops measured at 30 K for the four samples of Fig. 1, with the applied field perpendicular (—) and parallel to the film plane (- -).

radiation have confirmed the existence of such anisotropic local order [13].

4. Discussion

The chemical LRO along the growth direction observed in the $Co_{82}Pt_{18}$ film (sample a) results in a stacking of alternate Pt-rich and Pt-poor planes whose Pt compositions are an average equal to 28 and 8 at%. Such ordering is really different from that established in the FCC $L1_2$-type ordered Co_3Pt phase [2] or in the HCP DO_{19}-type ordered A_3B compounds (such as Co_3Mo or Co_3Nb) [14], since along the [1 1 1] or [0 0 0 1] direction, all the planes have the same A_3B composition. Therefore this uniaxial ordering is promoted by the MBE technique and is established along the advancing surface during the co-deposition of Co and Pt atoms.

We suggest that two effects would drive this LRO. The first effect is the segregation of Pt at the advancing surface. This point is supported by two recent studies reported in the literature: (i) a crystallographic LEED analysis which has revealed at the (1 1 1) surface of a random FCC $Co_{20}Pt_{80}$ single crystal the existence of a pure Pt segregated top layer and an oscillatory composition profile through the second and third underlying planes [15]; (ii) resonant surface magnetic X-ray diffraction measurements on the (1 1 1) surface of a ferromagnetic Co_3Pt alloy which have shown a reduction of Pt magnetic moment on the top layer also related to a reduced Co concentration [16]. The second mechanism is based on a dominant surface diffusion process compared to bulk diffusion in the temperature range which favors LRO. This is suggested by the values of the relaxation times τ for LRO determined in $CoPt_3$ bulk alloy [17], which decrease from 170 h (i.e much longer than the deposition time) to 8 h, as the temperature increases from 690 to 800 K. Thus driven by these two effects, the difference of composition between the two

uppermost atomic layers is successively frozen as the free surface advances, i.e the alloy film can be seen as a stacking of surface alloys.

On increasing the growth temperature, the atomic diffusion in the bulk increases and tends to annihilate the atomic arrangements at the free surface as well as in the buried layers. Inversely if the growth temperature is relatively low, surface diffusion is then too weak for favoring surface arrangements between Co and Pt atoms. Therefore, there exists a growth temperature, found around 690 K, which maximizes the uniaxial chemical ordering. Such behavior was recently described by a simple model based on both bulk and surface effects (diffusion and interactions) which reproduces quite well the growth temperature dependence of LRO in both Co_3Ru and $\sim Co_3Pt$ films [19]. From this model, the activation energies for bulk and surface diffusion, E_b and E_s, together with a maximum chemical long-range order parameter S_{max} (corresponding to the equilibrium value near the free surface) were obtained for Co_3Pt films: $E_b = 2.5 \pm 1$ eV, $E_s = 0.39 \pm 0.06$ eV and $S_{max} = 0.65$. The value of E_b is in relatively good agreement with those found in $L1_2$-type ordered $CoPt_3$ bulk alloys of 3.1 eV deduced from LRO kinetics [17] and in ordered $L1_0$-type CoPt films of 2.1 eV [18]. S_{max}, which is close to the maximum value of 0.63 found in the $Co_{77}Pt_{23}$ films grown on sapphire [9], is therefore not equal to 1 indicating that alternate pure Co and mixed (Co,Pt) planes cannot be achieved by the MBE process, due to weak bulk diffusion.

The stability of the chemically ordered Co_xPt_{1-x} films has been investigated through ex situ annealing treatments applied to the most ordered film (sample a) at the same temperature as its deposition temperature. Fig. 7 shows the change in the (0 0 0 1) superstructure peak with annealing time, measured on the HR Philips diffractometer. The chemical long-range order parameters deduced from the ratio $I_{0\,0\,0\,1}/I_{0\,0\,0\,2}$ are equal to 0.43 and 0.1 for annealing times equal to 6 h and one week. We have checked that there is no noticeable change in the volume fractions of HCP and FCC stackings in the annealed films. It appears clearly that the uniaxial chemical ordering promoted by the MBE technique is metastable, since it disappears

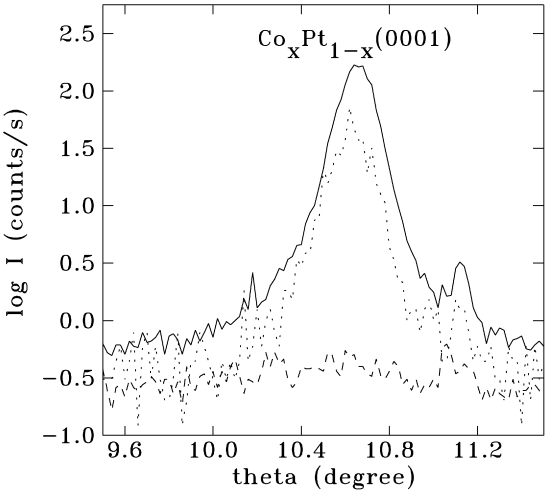

Fig. 7. Effect of ex situ annealing on the 0 0 0 1 peak measured in the $Co_{82}Pt_{18}$ film grown at 690 K (sample a) on the HRXRD diffractometer: as-deposited (—), annealed at 690 K for 6 h (....) and one week (- - -).

progressively with annealing time. Together with the decrease of chemical ordering, we observe a small increase in the distance between (0 0 0 1) planes of about 5×10^{-3} Å. The atomic rearrangements, which take place during annealing, are now driven by the only bulk interactions and the alloy film evolves towards its equilibrium state.

This result is in agreement with the total energy calculations carried out for three different structures of the Co_3Pt compound, namely $L1_2$, DO_{19} and DO'_{19} [20]. The labelled DO'_{19} structure is a modified form of DO_{19} which yields chemical ordering along the *c*-axis observed in the epitaxial films, i.e in the two alternate planes *A*–*B* along *c*, one plane contains only Co atoms. From these calculations, based on a TB-LMTO method, the ferromagnetic DO'_{19} phase is the least stable, while the most stable is the ferromagnetic DO_{19} phase. From long-time annealing, it should be possible to confirm whether the Co_xPt_{1-x} films evolve towards the DO_{19} structure foreseen by the theory, instead of the $L1_2$ structure already observed in a bulk Co_3Pt alloy [2].

Fig. 8 displays the decrease of *S* with annealing time found in sample a. As indicated by the dashed curve, such a decrease cannot be described by

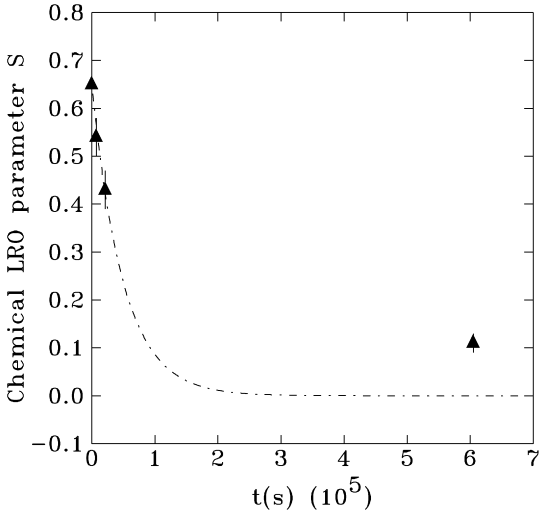

Fig. 8. Decrease of the chemical long-range order parameter as a function of the annealing time in the $Co_{82}Pt_{18}$ film grown at 690 K (sample a). For $t = 0$, $S = 0.65$, i.e. the equilibrium value at the free surface from Ref. [19]. Here, the description by a simple exponential law (dotted curve) is not valid (see also text).

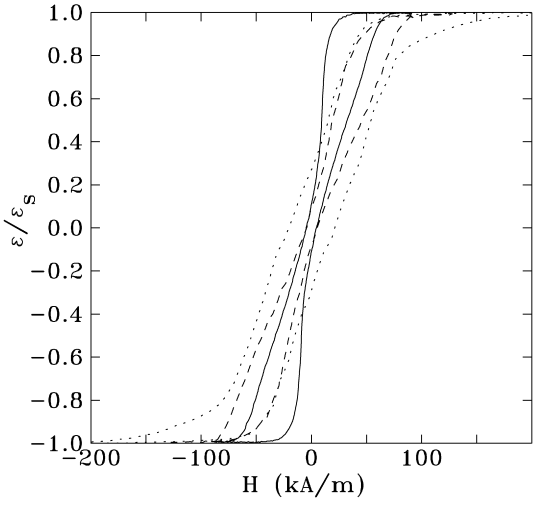

Fig. 9. Polar Kerr hysteresis loops measured at 300 K in the as-deposited $Co_{82}Pt_{18}$ film grown at 690 K (sample a) (—), and after ex situ annealing at 690 K for 6 h (- - -) and one week (....).

a simple exponential law in the whole annealing time range, such as $S = S_{max} \exp(-t/\tau)$, where τ is a relaxation time. Thus, this behavior differs from the relaxation process observed in bulk $CoPt_3$ when returning to its equilibrium ordered state. The dashed curve, which fits relatively well the S values for short times, corresponds to a relaxation time of 5×10^4 s, i.e. much shorter than that obtained for LRO in bulk $CoPt_3$ about 10^9 s. This deviation could be related to the existence of a vacancy supersaturation at the vicinity of defects (such as grain boundaries or dislocations), which disappears progressively during the anneal time. Therefore, the change of S over long times should be described at least by a longer relaxation time, that would be the equilibrium time. The decrease of chemical ordering in the annealed film modifies significantly its magnetic properties, as illustrated by the polar Kerr effect loops measured at 300 K (Fig. 9). Thus, a regular increase of the saturation field is observed together with a significant increase of the coercivity after long-time annealing. Such an increase of coercivity would be due to a separation of magnetic domains by non-magnetic regions, as for example the existence of Pt- or Ru-enriched regions localized at the grain boundaries where Ru buffer or Pt cap layer can diffuse preferentially. In fact, these (Pt,Ru)-enriched regions contribute to a shoulder on the left side of the (0 0 0 2)Ru peak in the X-ray pattern of the long-time annealed film and represent $\sim 1.5\%$ of the alloy volume. The uniaxial magnetic anisotropy for the film annealed at 690 K for one week, deduced from the SQUID magnetization loops is equal to 1 MJ/m^3, and becomes close to the value of pure HCP Co. Therefore, from these annealing treatments, a decrease of the chemical LRO parameter from 0.54 to 0.1 (corresponding to a decrease of the CoPt pairs oriented out of the film plane), leads to a strong decrease of the uniaxial anisotropy from 2.6 to 1 MJ/m^3.

In conclusion, we have shown that the predominantly HCP $\sim Co_{80}Pt_{20}$ films grown on Ru(0 0 0 1) buffer using a mica substrate can exhibit chemical LRO along the growth direction, characterized by alternate Co-rich and Co-poor planes. In contrast, no chemical ordering in the (0 0 0 1) planes was observed. This ordering, strongly dependent on the growth temperature and also on the crystalline quality of the film, enhances perpendicular magnetic anisotropy, characterized by uniaxial anisotropy energies up to 2.6 MJ/m^3 as found in

a highly chemically ordered $Co_{82}Pt_{18}$ film grown at 690 K. Yet, after ex situ annealing performed at the same temperature as the growth temperature, the uniaxial ordering strongly decreases together with a large decrease of perpendicular anisotropy. This result indicates that in agreement with theoretical calculations [20], the MBE-promoted low-temperature chemically ordered alloy is metastable. Both Pt segregation at the advancing surface and associated dominant surface diffusion during co-deposition at temperatures close to 690 K are suggested to be the driving effects of such unexpected chemical ordering effects in alloy films close to the Co_3Pt composition. On the contrary, in equiatomic (0 0 1)CoPt films grown on a (0 0 1) orientated substrate, a similar mechanism would favor the formation of the tetragonal $L1_0$-type ordered equilibrium phase, as found in Ref. [8].

Acknowledgements

We thank J. Arabski for the MBE growth of the samples and G. Schmerber for the annealing treatments.

References

[1] D. Weller, in: H. Ebert, G. Schütz (Eds.), Spin Orbit Influenced Spectroscopies of Magnetic Solids, Lecture Notes in Physics, Vol. 466, Springer, Berlin, 1996, p. 1.
[2] C. Leroux, M.C. Cadeville, V. Pierron-Bohnes, G. Inden, F. Hinz, J. Phys. F 18 (1988) 2033.
[3] J.M. Sanchez, J.L. Moran-Lopez, C. Leroux, M.C. Cadeville, J. Phys.: Condens. Matter 1 (1989) 491.
[4] C. Meneghini, M. Maret, M.C. Cadeville, J.L. Hazemann, J. Phys. IV France 7 C2 (1997) 1115.
[5] M. Maret, M.C. Cadeville, R. Poinsot, A. Herr, E. Beaurepaire, C. Monier, J. Magn. Magn. Mater. 166 (1997) 45.
[6] P.W. Rooney, A.L. Shapiro, M.Q. Tran, F. Hellman, Phys. Rev. Lett. 75 (1995) 1843.
[7] W. Grange, J.P. Kappler, M. Maret, J. Vogel, A. Fontaine, F. Petroff, G. Krill, A. Rogalev, J. Goulon, M. Finazzi, N. Brookes, J. Appl. Phys. 83 (1998) 6617.
[8] G.R. Harp, D. Weller, T.A. Rabedeau, R.F.C. Farrow, R.F. Marks, Mater Res. Soc. Symp. Proc. 313 (1993) 493.
[9] G.R. Harp, D. Weller, T.A. Rabedeau, R.F.C. Farrow, M.F. Toney, Phys. Rev. Lett. 71 (1993) 2493.
[10] M. Maret, M.C. Cadeville, W. Staiger, E. Beaurepaire, R. Poinsot, A. Herr, Thin Solid Films 275 (1996) 224.
[11] M. Maret, C. Ulhaq-Bouillet, W. Staiger, M.C. Cadeville, S. Lefebvre, M. Bessière, Thin Solid Films 319 (1998) 191.
[12] C.J. Lin, G.L. Gorman, C.H. Lee, R.F.C. Farrow, E.E. Marinero, H.V. Do, H. Notarys, C.J. Chien, J. Magn. Magn. Mater. 93 (1991) 194.
[13] C. Meneghini, M. Maret, V. Parasote, M.C. Cadeville, J.L. Hazemann, R. Cortes, S. Colonna, Eur. Phys. J. B (1998), in press.
[14] P. Villars, L.D. Calvert, Pearson's Handbook of Crystallographic Data for Intermetallic Phases, vol. 2, American Society for Metals, Cleveland, OH, 1985.
[15] Y. Gauthier, R. Baudoing-Savois, J.M. Bugnard, U. Bardi, A. Atrei, Surf. Sci. 276 (1992) 1.
[16] S. Ferrer, P. Fajardo, F. de Bergevin, J. Alvarez, X. Torrelles, H.A. Van der Vegt, V.H. Etgens, Phys. Rev. Lett. 77 (1997) 747.
[17] C.E. Dahmani, M.C. Cadeville, V. Pierron-Bohnes, Acta Metall. 33 (1985) 269.
[18] D.M. Artymowicz, B.M. Lairson, B.M. Clemens, J. Crystal Growth 169 (1996) 83.
[19] L. Bouzidi, V. Pierron-Bohnes, O. Haemmerlé, C. Ulhaq-Bouillet, M.C. Cadeville, Thin Solid Films 318 (1998) 215.
[20] G. Moraïtis, J.C. Parlebas, M.A. Khan, J. Phys.: Condens. Matter 8 (1996) 1151.
[21] W. Grange, J.P. Kappler, M. Maret, J. Vogel, A. Fontaine, F. Petroff, G. Krill, A. Rogalev, J. Goulon, M. Finazzi, N. Brookes, Phys. Rev. B 58 (1998) 6298.